

https://dspace.org/

Assessing vulnerability to embolism and hydraulic safety margins in reedlike Restionaceae

A G West; K Atkins; J J van Blerk; Robert Skelton

WILEY-BLACKWELL
https://hdl.handle.net/10539/43064
WOS

Downloaded from a DSpace repository. https://dspace.org/

plant biology

Plant Biology ISSN 1435-8603

RESEARCH ARTICLE

Assessing vulnerability to embolism and hydraulic safety margins in reed-like Restionaceae

A. G. West[1], K. Atkins[1], J. J. van Blerk[1] & R. P. Skelton[2,3]

1 Department of Biological Sciences, University of Cape Town, Rondebosch, South Africa
2 Fynbos Node, South African Environmental Observation Network, Newlands, South Africa
3 Department of Animal, Plant and Environmental Sciences, University of the Witwatersrand, Johannesburg, South Africa

Keywords
Embolism; graminoids; optical method; P_{50}; pneumatron; Restionaceae; turgor loss point.

Correspondence
A. G. West, Department of Biological Sciences, University of Cape Town, Rondebosch, South Africa.
E-mail: adam.west@uct.ac.za

Editor
C. Werner

Received: 30 November 2023;
Accepted: 12 March 2024

doi:10.1111/plb.13644

ABSTRACT

- The African Restionaceae (Poales), the dominant graminoid layer in the megadiverse Cape Floristic Region of South Africa, are distributed across a wide range of moisture availability, yet currently there is very little known about the underlying hydraulics of this group.
- We tested two methods for measuring culm vulnerability to embolism, the optical and pneumatic methods, in three species of *Cannomois* ranging in habitat from semi-riparian (*Cannomois virgata*) to dryland (*Cannomois parviflora* and *C. congesta*). Estimates of culm xylem vulnerability were coupled with measures of turgor loss point (Ψ_{TLP}) and minimum field water potential (Ψ_{MD}) to assess hydraulic safety margins.
- The optical and pneumatic methods produced similar estimates of P_{50}, but differed for P_{12} and P_{88}. All three species were quite vulnerable to embolism, with P_{50} of −1.9 MPa (*C. virgata*), −2.3 MPa (*C. congesta*), and −2.4 MPa (*C. parviflora*). Estimates of P_{50}, Ψ_{TLP} and Ψ_{MD} aligned with habitat moisture stress, with highest values found in the semi-riparian *C. virgata*. Consistent differences in P_{50}, Ψ_{MD} and Ψ_{TLP} between species resulted in consistent hydraulic safety margins across species of 0.96 ± 0.1 MPa between Ψ_{MD} and P_{50}, with onset of embolism occurring 0.43 ± 0.04 MPa after Ψ_{TLP} for all three species.
- Our study demonstrates that restio occupancy of dry environments involves more than the evolution of highly resistant xylem, suggesting that other aspects of water relations are key to understanding trait–environment relationships in this group.

INTRODUCTION

Graminoids are a highly diverse and ecologically important group of plants, influencing ecosystem productivity structure (Bond & Midgley 2012; February *et al.* 2013), distribution (Staver *et al.* 2011), drought sensitivity (Knapp *et al.* 2002; Craine *et al.* 2013; Van Sundert *et al.* 2021), carbon storage (Goud *et al.* 2022; Zhou *et al.* 2022), herbivore abundance (Staver *et al.* 2019) and fire regimes (Karp *et al.* 2021) globally. The tolerance of graminoids to environmental stress is an important factor influencing their productivity (Fay *et al.* 2003) and distribution (Jurjavcic *et al.* 2002). A critical environmental stress is water availability, with both a surfeit and deficit of water presenting stressful conditions that can differentially affect co-occurring species (Swemmer *et al.* 2006), and structure communities (Silvertown *et al.* 1999; Araya *et al.* 2011; Silvertown *et al.* 2015). Climate models predict an intensification of the water cycle in future, increasing the frequency and duration of drought and flooding events globally (IPCC 2022), making understanding the tolerance of moisture extremes in graminoids increasingly important.

A key trait for drought tolerance in plants is the resistance of the xylem to embolism and hydraulic failure (Tyree & Sperry 1989). Under severe drought stress, plant water potentials can fall low enough to induce air to enter the xylem of the plant, causing emboli that disrupt water transport and can result in desiccation and death of the plant through hydraulic failure (McDowell *et al.* 2008; Brodribb *et al.* 2021). Hydraulic failure is thought to be the main cause of drought-related woody plant mortality globally (Anderegg *et al.* 2012; Adams *et al.* 2017; Choat *et al.* 2018) and has received considerable attention in the literature (Choat *et al.* 2018; Brodersen *et al.* 2019; Brodribb *et al.* 2020). However, compared to woody plants, relatively little is known about the importance of hydraulic failure in graminoids. There are reasons to assume that hydraulic failure might be a less important trait for graminoids than woody plants because of the lower investment in biomass supporting the photosynthetic tissue, as well as the ability of some graminoids to escape drought phenologically, to resprout or to potentially refill embolized vessels by positive xylem pressure (Holloway-Phillips & Brodribb 2011; Cao *et al.* 2012). However, recent work suggests that there is considerable variation in graminoid physiological drought tolerance (Craine *et al.* 2013) and resistance to embolism (Jacob *et al.* 2022) that is comparable to that of woody plants (Lens *et al.* 2016). As such, hydraulic failure, or the avoidance thereof, may be an important factor influencing crop resilience (Corso *et al.* 2020), graminoid productivity (Jacob *et al.* 2022) and structuring communities (Ocheltree *et al.* 2020), warranting further research into the hydraulic traits of graminoids globally.

This is an open access article under the terms of the Creative Commons Attribution-NonCommercial-NoDerivs License, which permits use and distribution in any medium, provided the original work is properly cited, the use is non-commercial and no modifications or adaptations are made.

The Restionaceae (hereafter "restios") are reed-like monocots that constitute the bulk of the graminoid layer in the mega-diverse sclerophyllous Fynbos Biome of the Cape Floristic Region (CFR) in southwestern Africa (Rebelo *et al.* 2006). The restios differ from grasses in that they have photosynthetic culms rather than leaves, and cluster roots rather than mycorrhizal symbionts (Bell *et al.* 2000), and appear to dominate the more nutrient-poor soils of the region (Goldblatt 1978; Campbell 1983; Bond & Goldblatt 1984; Hoffman *et al.* 1987; Bergh *et al.* 2014).

The restios represent a fascinating graminoid group to explore hydraulically. The 350 species of African restios are well resolved phylogenetically (Briggs & Linder 2009) and occur across the full hydrological range in the fynbos, from the lowest rainfall on well-drained sand to the highest rainfall or perennially waterlogged habitats (Born & Linder 2018). Additionally, they have been shown to be strongly segregated by moisture availability patterns across small scales, with the proportion of time spent under flooding-induced or drought-induced stress correlating with species occurrence (Araya *et al.* 2011; Araya *et al.* 2012) and forming part of the fundamental niche (Born & Linder 2018). The ability to tolerate flooding stress has been well linked to the presence of aerenchymatous roots in the restios (Huber & Linder 2012), however less attention has been paid to the adaptations and trade-offs associated with coping with drought-related stress in this group, and the extent to which this relates to fundamental and realized niches. Interestingly, restios in mesic mountain fynbos have been shown to be remarkably drought resistant (West *et al.* 2012), maintaining high water potentials and low rates of transpiration over the dry summer (Skelton *et al.* 2023) despite being shallow rooted (West *et al.* 2012; Skelton *et al.* 2023); a phenomenon that has been attributed to their ability to utilize cloud (Marloth 1903, 1905; Nagel 1956) and dew moisture (Skelton *et al.* 2023) during rain-free periods. However, the broad environmental range, and considerable lability in root architecture (Ehmig & Linder 2020) of the restios, demand that traits relating to drought stress are more widely investigated in this group. An important step towards this, is the development of a reliable method of measuring drought-related vulnerability to embolism in this group.

Here we test two methods of obtaining estimates of xylem vulnerability to drought-induced embolism for restio culms. The morphology of these culms, with sparsely distributed vascular bundles embedded in ground tissue, often with a central cavity (Fig. 1), presents a potential challenge for obtaining reliable estimates of vulnerability to embolism. We derived estimates of vulnerability to embolism using the optical vulnerability method (Brodribb *et al.* 2016; Brodribb *et al.* 2017) and the automated pneumatic method, or 'pneumatron' (Pereira *et al.* 2016, 2020). The optical method has been used successfully on graminoid leaves previously (e.g., Johnson *et al.* 2018; Corso *et al.* 2020; Jacob *et al.* 2022), but is yet to be tested on graminoid shoots or culms. An advantage of the optical method is that it is able to directly assess xylem embolism through image analysis (Jacob *et al.* 2022). In contrast, the pneumatic method relies on the assumption that air discharged under a mild vacuum from an attached plant segment is proportional to the amount of xylem embolism that segment has experienced (Pereira *et al.* 2016; Yang *et al.* 2022; Paligi *et al.* 2023). The pneumatic method has been used successfully to generate xylem vulnerability curves in a wide range of woody angiosperm species, including leaves (Pereira *et al.* 2020), but it has yet to be tested on graminoid shoots or culms. It is possible that gas diffusion from non-xylary tissues, or changes in volume during dehydration, may obscure gas diffusion from embolized xylem in graminoid culms. As such, this method may not be well suited to measuring xylem embolism in restioid culms that may distort or collapse during dehydration. Yet, the relative ease and simplicity of the technique demands that it be tested.

We chose three restio species of the genus *Cannomois* P.Beauv. ex Desv. from a range of habitats, from riparian to dryland, to test our methods. We measured vulnerability to embolism using the optical and pneumatic methods, minimum seasonal water potentials in the field (Ψ_{min}) and pressure–volume curves. We hypothesized that culm xylem would embolise at lower water potentials than those associated with turgor loss point and regular seasonal *in situ* moisture stress in all species, and that vulnerability to embolism would be correlated with environmental conditions (more vulnerable in wetter habitats). We inferred that the creation of realistic vulnerability curves, with agreement across the methods and traits, would indicate that hydraulic trait measurements can be successfully obtained in restio culms and can be applied more broadly within the Restionaceae and across other morphologically similar graminoid species.

MATERIAL AND METHODS

Sample selection and collection

The study was conducted on three common species of Restionaceae from the *Cannomois* genus representing a range of habitats and environmental conditions across the Cape Floristic Region. Species descriptions below were taken from Linder (2018). *Cannomois virgata* (Rottb.) Steud. is mostly found on south-facing slopes between 30 and 1800 m, in mesic areas with relatively high rainfall or in valley bottom seeps. Plants are 1.0–1.5-m tall with a well-developed spreading rhizome and large culms between 7.5 and 10.0 mm in diameter. Culms are robust, with five to eight thick-walled sclerenchyma layers, and a central ground tissue containing a central cavity. For this study, female plants were sampled from a steep south-facing slope adjacent to a river, in Jonkershoek Nature Reserve (33°58.4′ S, 18°56.5′ E, 270 m a.s.l., 1600 mm MAP). *Cannomois congesta* Mast. is mostly found on well-drained pebbly or sandy soils between 1100 and 2000 m. Plants are 0.5–1.0-m tall, compact, without spreading rhizomes, and culms approximately 1–2 mm in diameter. Culms have three to six thin-walled sclerenchyma layers, and a central cavity. For this study, female plants were sampled from a flat, sandy plain at Jonaskop (33°56.5′ S, 19°31.5′ E, 990 m a.s.l., 500 mm MAP). *Cannomois parviflora* (Thunb.) Pillans incorporates numerous synonyms, including *Cannomois acuminata* (Kunth.) Pillans. It is mostly found on well-drained pebbly or sandy soils between 150 and 1500 m. Plants are 0.5–1.0-m tall, with spreading rhizomes, and culms approximately 1–2 mm in diameter. Culms have four to six thick-walled sclerenchyma layers, and central ground tissue with scattered cavities or a central cavity. For this study, female plants were sampled from a NE-facing pebbly slope at Algeria in the Cederberg (32°22.4′ S, 19°3.2′ E,

14388677, 2024, 4, Downloaded from https://onlinelibrary.wiley.com/doi/10.1111/plb.13644 by University Of Witwatersrand, Wiley Online Library on [22/11/2024]. See the Terms and Conditions (https://onlinelibrary.wiley.com/terms-and-conditions) on Wiley Online Library for rules of use; OA articles are governed by the applicable Creative Commons License

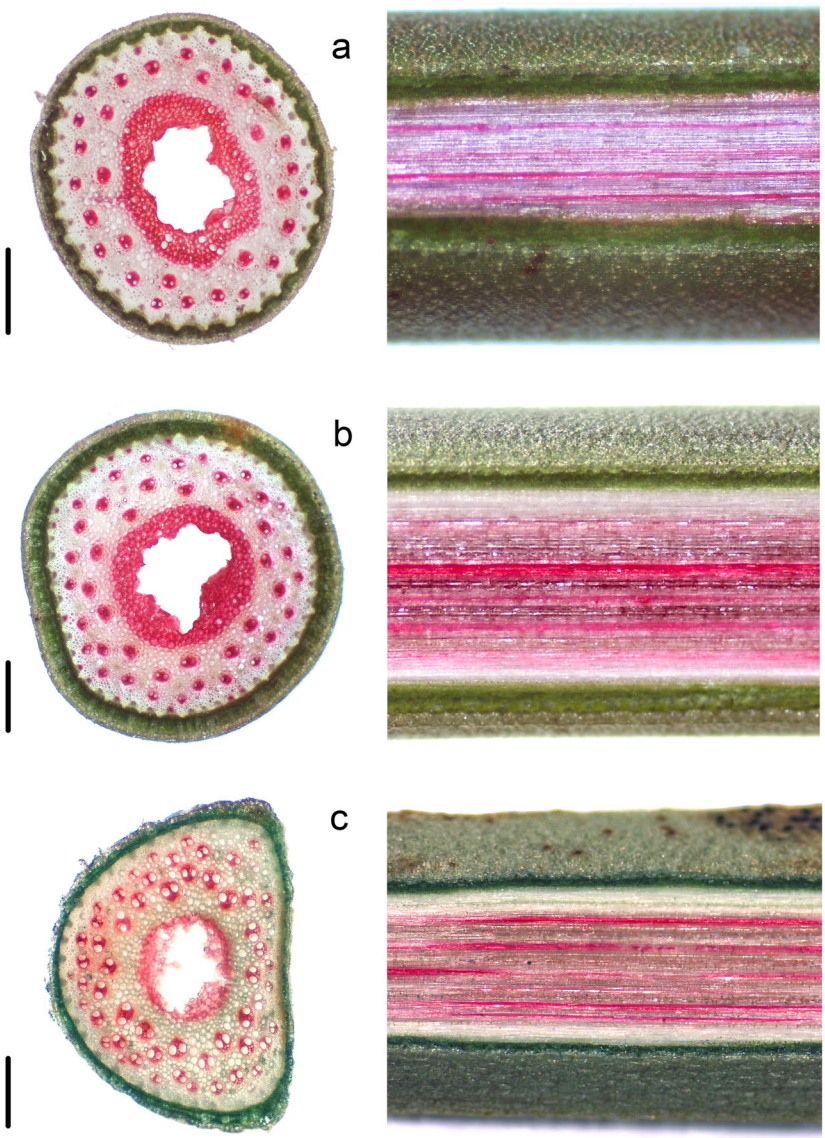

Fig. 1. Cross- and transverse sections of culms showing vascular bundles for *Cannomois parviflora* (a), *C. congesta* (b) and *C. virgata* (c). Vascular bundles were stained by perfusing safranin dye through the culm. Note the presence of large central cavity. Transverse sections show the "window" cut for the optical vulnerability technique, exposing the xylem embedded within the collenchyma, by removing the epidermal layers. Scale bar = 0.5 mm.

550 m a.s.l., 675 mm MAP). A plant water relations study in this location in the 1980s (Miller *et al.* 1984) identified this species as *Cannomois accuminata* (Kunth) Pillans, which is now a synonym for *C. parviflora* (Linder 2018).

We collected entire rhizomes, with culms attached, from at least three healthy female individuals of each species. Care was taken to keep the plant intact when sampling so as not to induce any embolism into the culms. Rhizomes were placed in large plastic bags with damp paper towels, which were then sealed to prevent further water loss while being transported to the laboratory for processing. Two sampling periods were conducted. The first, in October 2021, sampled plant material for optical vulnerability curves. The second sampling period, in June 2022, sampled material for pressure–volume curves and pneumatic vulnerability curves. Identical methods were followed in both sampling campaigns, and the same populations were sampled.

Field xylem water potential

Predawn and midday xylem water potentials were measured on at least four individuals of each species in the field during February and March 2021 using a Scholander-type pressure chamber (PMS Instruments, Corvallis, Oregon, USA). Midday measurements were made between 12:00 and 14:00 h and predawn measurements were made approximately 1 h before sunrise. For each measurement, a single, fully developed culm was excised and then wrapped in moist paper towel and placed in a plastic bag to prevent further water loss while being measured.

14388677, 2024, 4, Downloaded from https://onlinelibrary.wiley.com/doi/10.1111/plb.13644 by University Of Witwatersrand, Wiley Online Library on [22/11/2024]. See the Terms and Conditions (https://onlinelibrary.wiley.com/terms-and-conditions) on Wiley Online Library for rules of use; OA articles are governed by the applicable Creative Commons License

Culm anatomy and vessel length

To examine the xylem anatomy in our species, the xylem of a representative culm of each species was stained with 0.1% aqueous safranin dye solution in distilled water. Culm sections spanning two nodes (i.e., consisting of one full intact internode) were cut underwater using a single-edged carbon steel blade. The basal end of the section was attached to a 5 ml syringe, containing dye, and pressure was applied until a steady flow of dye came out the distal end. Thereafter, the segments were flushed with water until the water ran clear of excess dye. A window of epidermis and chlorenchyma tissue was carefully removed in the same way a culm would be prepped for optical scanning (see "Optical vulnerability measurements" below) to expose stained xylem tissue. Cross-sections were taken by hand sectioning. Lateral and cross-sectional images were captured using a dissecting microscope (Lecia EZ4 HD). To test whether vessels and the hollow central cavity spanned nodes, we perfused pressurized air (100 kPa) into the proximal end of a culm while placing the distal end into a bucket of water. The distal end was then progressively cut back until bubbles could be seen streaming from the cut surface. For all species, vessels and the central cavity did not span the nodes. Thus, for pneumatic measurements, culms were excised just below the most basal node. This eliminated the concern of open vessels spanning the culm and minimized the air volume of the open central cavity.

Optical vulnerability measurements

We used the optical method described in Brodribb *et al.* (2016), Brodribb *et al.* (2017), and Skelton *et al.* (2018) to generate xylem vulnerability curves for restioid culms. Full details of the method, including an overview of the technique, image processing, as well as scripts to guide image capture and analysis, are also available at http://www.opensourceov.org.

We attached culms, still attached to the rhizome, to flatbed scanners (Epson perfection V800 or V850 Scanner, Epson USA) to generate a time series of images of an exposed section of the xylem within the culm as the entire plant desiccated over a few days. We measured a single culm per individual plant (n = 3 individuals) for both *C. virgata* and *C. parviflora*. For *C. congesta*, we measured three culms per individual, for three individuals. The three culms per individual were subsequently averaged per individual (resulting in n = 3 individuals). The xylem was exposed by carefully removing the epidermal and chlorenchymal layer from a small section of the culm, using a dissecting microscope and a single-edged carbon-steel blade (Fig. 1). During this procedure, considerable care was taken to not cut any xylem tissue and to ensure that the exposed vascular tissue remained moist by periodically dousing it in water to prevent any air entering the xylem before measurement. The culm was then attached to the scanner with the window of exposed xylem tissue facing down. Each window was surrounded by a rectangular putty (Prestik, Bostik, SA) frame to create a containment well for ultrasound gel (Tensive ultrasound gel; Parker Labs, America). The ultrasound gel ensured that the window did not desiccate too rapidly without impeding the transmission of light to the xylem surface. Each well was then covered by a glass microscope slide and was secured to the scanner bed with duct tape to prevent any movement which may interfere with measurements during the dry down process. Culms were then scanned in reflective mode at 4800 dpi every 5 min over a period of a few days, allowing us to track embolism events over time within the xylem in each sample.

Concurrently to optical scanning, we measured the decline in xylem water potential of culms attached to the same rhizome as the scanned culms using a Scholander-type pressure chamber (PMS Instruments, Corvallis, OR, USA). Culm water potential was periodically measured until the water potential fell too low for reliable pressure chamber measurements for these species (between −2 and −3 MPa). This related to a minimum water potential measurement equal to or less than P_{50} for all species. The optical measurements where then continued for at least 36 h after this point until the culms were visibly desiccated and discoloured.

Upon completion, image sequences were analysed to identify embolism events, seen as changes in the reflection of the stem xylem. Image subtraction of subsequent images conducted in ImageJ (National Institutes of Health, Bethesda, MD, USA) was used to reveal rapid changes in light transmission or contrast produced by each embolism event. Slow movements of the culms caused by drying could easily be distinguished from embolism events and were filtered from the analysis. Embolism events were thresholded, allowing automated counting of each event using the analyse-stack function in ImageJ. From the thresholded stack of embolism events we could extract a time-resolved count of embolism events (using the timestamp of each image). We then converted the raw embolism counts to a percentage of total pixels embolized, producing a dataset of time-resolved percentage embolism. The time-resolved percentage embolism data were combined with the xylem water potential timeline to estimate the culm xylem water potential associated with each embolism event. The water potential data were modelled using segmented regressions that described the rapid initial phase of water potential decline to turgor loss point, followed by a more gradual secondary decline. This secondary decline was then extrapolated to match the end of the optical data time series. Vulnerability to embolism was recorded as the relationship between percentage embolism and water potential (Ψ), and modelled using a sigmoid function (Pammenter & van Wiligen 1998):

$$\text{Percentage embolism} = \frac{100}{(1 + e^{a(\Psi - b)})} \quad (1)$$

where a corresponds to the sensitivity to decreasing water potential (proportional to the slope of the equation) and b is the water potential associated with 50% embolism (P_{50}, MPa). P_{88} and P_{12} were calculated using the equations of Domec & Gartner (2001). 95% confidence limits of the vulnerability curves were calculated through bootstrapping.

Pneumatic vulnerability measurements

We constructed automated 'pneumatrons', with ports for two culms, programmed to measure the air discharge from the attached culms every 15 min following the protocol of Pereira *et al.* (2020) and Trabi *et al.* (2021). Individual culms were excised from field-collected plants that were being kept in large, moistened plastic bags in the laboratory. Every effort

14388677, 2024, 4, Downloaded from https://onlinelibrary.wiley.com/doi/10.1111/plb.13644 by University Of Witwatersrand, Wiley Online Library on [22/11/2024]. See the Terms and Conditions (https://onlinelibrary.wiley.com/terms-and-conditions) on Wiley Online Library for rules of use; OA articles are governed by the applicable Creative Commons License

was made to prevent culm desiccation occurring prior to measurements commencing on the pneumatrons. Prior to excision from the plant, individual culms were placed in smaller plastic bags with moist paper towel and sealed basally. This was done inside the larger plastic bag containing the entire plant. The culm was then excised at the base and connected directly to a port on a pneumatron using tight-fitting silicon tubing. Experimentation showed that leaks were best prevented using contact adhesive (Genkem) around the outside of the culm/-tube interface. The flexibility of the contact adhesive was sufficient to prevent leaks even as the culm shrunk during dry down. After all culms were attached, and the pneumatrons had gone through a few cycles to verify there were no leaks, the bags were removed from the culms, and the benchtop dry-down commenced.

Each measurement cycle commenced with pulling a vacuum on the culm that reduced the pressure in the manifold to approximately 30 kPa. The pressure in the discharge tube was then measured for 30 s, following which the tube was vented and returned to atmospheric pressure. Air discharge (AD, μl) was calculated, following the methods of Pereira *et al.* (2016, 2020), as:

$$AD = \left(\frac{(P_f - P_i) \times V_r}{P_{atm}}\right) \times 10^6 \quad (2)$$

where P_{atm} is atmospheric pressure (kPa), V_r is the discharge tube volume of the pneumatron (~0.001 l), P_i is the initial pressure (kPa), measured immediately after imposing the partial vacuum on the culm, and P_f is the final pressure (kPa), measured after 5 s. The 5-s timeperiod was empirically determined as yielding the best results, as longer times tended to result in greater noise and less differentiation in AD across the entire dry-down, possibly due to diffusion of air through the non-xylary components of the culm.

We ran two rounds of pneumatic measurements for each species, attempting to obtain sufficient culm replication. We aimed to measure three individual plants per species, with each individual plant represented by the average of two culms. However, several culms provided no coherent air discharge trend per round. For *C. congesta* and *C. parviflora* we obtained curves for three individual plants, but for *C. parviflora* we only recovered curves for two individuals. This would need to be improved upon for ecological studies seeking sufficient statistical power to detect small differences between species and populations. During each round of measurements, culm water potential was measured periodically on additional excised culms that were handled in as similar a manner to pneumatron culms as possible. These culms were excised at the same time as the pneumatron culms and were placed alongside the pneumatron culms in the laboratory to dry down together. Measurements were made and modelled in the same manner as described for the optical method above. Each water potential culm was only measured once, to prevent the possibility of cumulative damage skewing the water potential measurements over the course of the dry down.

The pneumatron measurements were terminated when the culms were visibly desiccated and discoloured and the air discharge curve had plateaued. At the conclusion of the dry-down, percent air discharge (PAD, %) was calculated as:

$$PAD = 100 \times \frac{(AD - AD_{min})}{(AD_{max} - AD_{min})} \quad (3)$$

where AD_{min} is the minimum and AD_{max} is the maximum amount of air discharge (μl) measured over the dry-down period. These time-resolved percentage air discharge data were combined with the xylem water potential (Ψ) timeline and modelled using a sigmoid function (Pammenter & van Wiligen 1998) as for the optical curves.

Pressure–volume curves

Pressure–volume curves were created for three culms per species by repeatedly measuring the xylem water potential (following the methods described above), together with the culm mass, as the culms desiccated from a fully hydrated state in the laboratory. Once the measurements were completed, the culms were dried at 60 °C for 48 h and then weighed to obtain the dry mass. The relative water content (RWC; %) was then calculated as:

$$RWC = \frac{m_w - m_d}{m_s - m_d} \times 100 \quad (4)$$

where m_w is the wet mass at any given time, m_d is the dry mass, and m_s is the saturated mass which was the first mass measurement taken on the culms when they were fully hydrated.

For each culm a pressure–volume curve was plotted as $-1/\Psi$ (MPa^{-1}) versus 100 – RWC (%) and the turgor loss point (Ψ_{TLP}; MPa), osmotic potential (Ψ_0), and relative water content at turgor loss point (RWC_{TLP}) were calculated using standard procedures (Nicotra *et al.* 2010; Bartlett *et al.* 2012).

Hydraulic safety margins

Hydraulic safety margins were calculated in two ways: $HSM_{\Psi MD}$ was calculated as the difference between minimum field water potential (Ψ_{MD}) and the P_{50} obtained from averaging the optical and pneumatic estimates. $HSM_{\Psi TLP}$ was calculated as the difference between the turgor loss point (Ψ_{TLP}) and the P_{50} obtained from averaging the optical and pneumatic estimates. Error was propagated as:

$$\varepsilon_{(A-B)} = \sqrt{(\varepsilon_A^2 + \varepsilon_B^2)} \quad (5)$$

where A and B are the two means being subtracted and ε is the error associated with that mean.

Statistical analyses

All analyses were performed using R Statistical Software (version 4.2.1; R Core Team 2022) and the "tidyverse" suite (Wickham *et al.* 2019). Segmented regressions were fit to optical and pneumatron dry-down water potential time series using the "segmented" package in R (version 1.6-0; Muggeo 2008). Sigmoid curves were fit to optical and pneumatron data using "nls" (R Core Team 2022). 95% confidence intervals of species mean curves were calculated by bootstrapping. Plots were produced using "ggplot2" (Wickham 2016) and "ggpubr" (Kassambara 2020). Differences in model parameters between

14388677, 2024, 4, Downloaded from https://onlinelibrary.wiley.com/doi/10.1111/plb.13644 by University Of Witwatersrand, Wiley Online Library on [22/11/2024]. See the Terms and Conditions (https://onlinelibrary.wiley.com/terms-and-conditions) on Wiley Online Library for rules of use; OA articles are governed by the applicable Creative Commons License

species, method and their interaction were tested for using two-way ANOVA and Tukey HSD post-hoc comparisons. Where a factor not significant in the full model, a reduced model, only containing the significant factors, was used following the procedures of Crawley (2012).

RESULTS

Culm anatomy with regard to optical and pneumatic methods

The three *Cannomois* species examined in this study all had culms with a similar anatomical structure, with distributed vascular bundles surrounded by parenchymatous tissue, and a large hollow cavity in center of the culm. Our staining showed that there was considerable xylem visible from the cleared epidermal layer (Fig. 1), suitable for a robust optical measurement. To date the pneumatic method has not been successfully applied to herbaceous monocots. However, as the pneumatic method normalizes air discharge through the course of a dry-down to the initial air discharge from the hydrated culm, the presence of a large fraction of parenchymatous tissue and a large central cavity are not necessarily problematic for this technique. Potential challenges are the sparse vascular bundles resulting in a small air discharge volume requiring a low volume discharge tube to obtain sufficient resolution (see Pereira *et al.* 2020), the potential for early gas discharge from residual water on the exposed cut surface (e.g., Miranda *et al.* 2023) and potential changes in the volume of airspace in the culm during the dry-down which could potentially obscure patterns of air discharge from the xylem.

Optical vulnerability curves

Xylem embolism events were readily discernable in the imagery as sharply defined lines (Fig. 2). In contrast, movement or collapse of non-xylary tissues resulted in more diffuse changes that were easy to differentiate from the xylem and thus exclude from the analysis. As the culms were still attached to intact rhizomes, the plants dried-down slowly, taking up to 6 days to complete the dry-down (Fig. 3). The culms for *C. congesta* and *C. virgata* dried-down at similar rates, evidenced by the similar progression of percentage embolism and water potential with time for each culm (Fig. 3b, c, e, f). As such, a single relationship between water potential and time was used to create the vulnerability curves for these species (Fig. 3h, i). For *C. parviflora*, it was apparent from both the optical and the water potential data that the progression of the dry-down was more rapid for one of the individuals than for the other two (Fig. 3a, d). As such, we fitted a separate water potential versus time relationship for this one individual. Doing so reduced the variation in vulnerability curves between the individuals (Fig. 3g), which we regarded as a more accurate reflection of variation between the individuals.

Pneumatic vulnerability curves

We obtained reasonable air discharge curves from the three species of *Cannomois* (Fig. 4). The larger, more rigid culms of *C. virgata* produced a greater gas discharge volume than the smaller, more flexible culms of *C. parviflora* and *C. congesta*. For the latter two species, pressure differences through the dry-down were small, despite minimizing the discharge tube volume to ±1 ml. This resulted in less resolution for the *C. parviflora* and *C. congesta* curves than for *C. virgata*. This could be improved in future by further minimizing discharge tube volume.

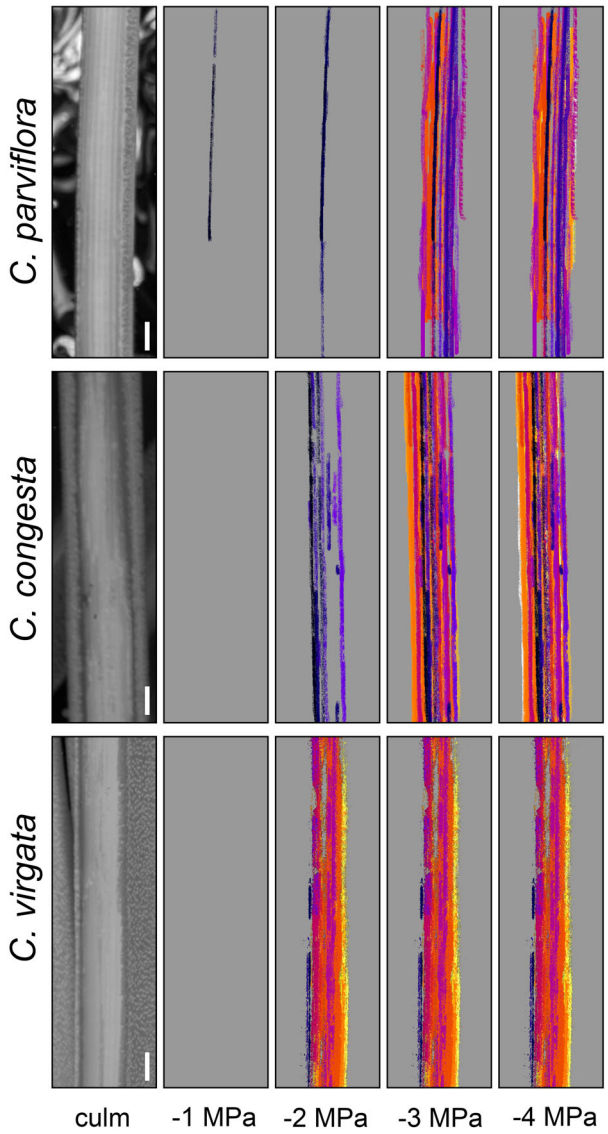

Fig. 2. Dehydration sequence of exposed culm xylem sections, for the optical technique, for three *Cannomois* species. In each row the first image depicts the culm with the exposed "window" showing xylem vessels. Subsequent images in each row depict cumulative embolism events in each culm, from fully hydrated to the given water potential. Emboli are coloured from earlier (colder/darker colours) to later events (warmer/lighter colours).

For the pneumatic method, the dry-down progressed much faster than for the optical method, as the culms were excised from the plant, rather than attached to the rhizomes. For both *C. parviflora* and *C. congesta*, the culms dried down at similar rates, as such a single relationship between water potential and time (Fig. 4d, e) was used to create the vulnerability curves for each of these species (Fig. 4g, h). For *C. virgata*, the culms were bagged overnight during the first measurement round (Fig. 4c), but not for the second round of measurements. As such, we used separate water potential versus time relationships

14388677, 2024, 4, Downloaded from https://onlinelibrary.wiley.com/doi/10.1111/plb.13644 by University Of Witwatersrand, Wiley Online Library on [22/11/2024]. See the Terms and Conditions (https://onlinelibrary.wiley.com/terms-and-conditions) on Wiley Online Library for rules of use; OA articles are governed by the applicable Creative Commons License

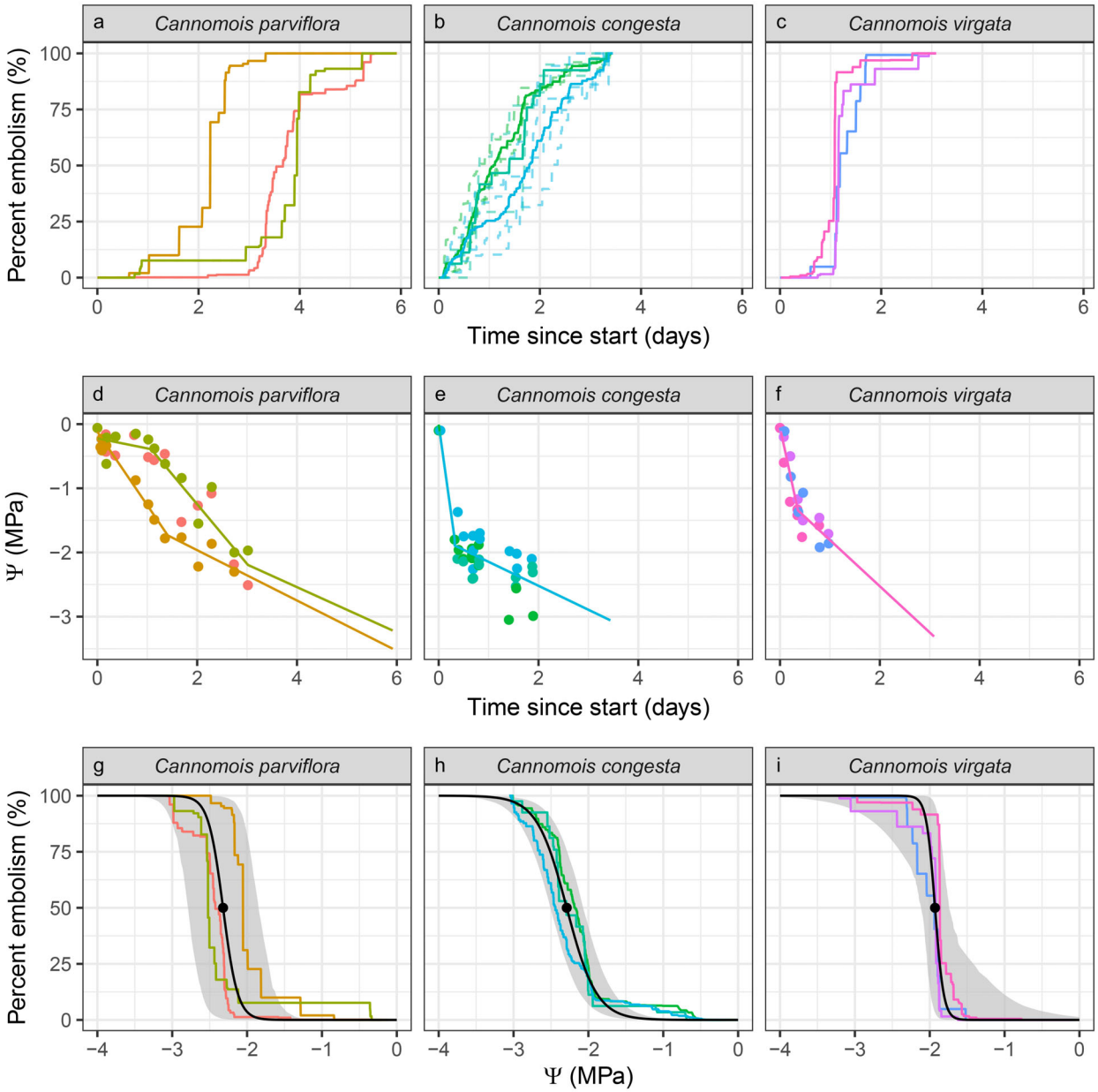

Fig. 3. Optical vulnerability curves for three *Cannomois* species. (a–c) Timeline of percentage embolism for each species, where each solid line represents an individual plant. For *C. congesta*, three culms (dashed lines) were averaged per plant (solid lines). (d–f) Timeline of water potential for each species. Points indicate observed values recorded using the Scholander-type pressure chamber, lines indicate interpolated xylem water potential (see Material and Methods for details). (h–j) Xylem vulnerability curves for each species. Coloured lines correspond to lines in (a–c), solid black lines are mean xylem vulnerability curves, filled black circles indicate the P_{50} values, and the grey shaded areas indicate 95% confidence intervals for each species.

for each measurement round for this species (Fig. 4g) to create the vulnerability curves (Fig. 4i).

Comparison of vulnerability curve methods

The optical and pneumatic methods produced similar estimates of P_{50} for all three species but differed for P_{12} and P_{88} (Tables 1 and 2, Fig. 5), with the pneumatron producing higher estimates of P_{12} and lower estimates of P_{88} than the optical method (Figs 5 and 6).

There was a strong species effect for both methods for P_{50}, P_{12} and P_{88} (Table 2, Fig. 5). For P_{50}, both methods produced a significantly higher P_{50} for *C. virgata* compared to *C. parviflora* and *C. congesta*, but no significant difference between *C. parviflora* and *C. congesta* (Fig. 5a). For P_{12}, the optical method produced no difference between the species, whereas the pneumatic method resulted in higher estimates of P_{12} for *C. congesta* and *C. virgata*, but not for *C. parviflora*, resulting in a significant *species:method* interaction (Fig. 5b). For P_{88}, both methods produced similar relative patterns for the species,

14388677, 2024, 4, Downloaded from https://onlinelibrary.wiley.com/doi/10.1111/plb.13644 by University Of Witwatersrand, Wiley Online Library on [22/11/2024]. See the Terms and Conditions (https://onlinelibrary.wiley.com/terms-and-conditions) on Wiley Online Library for rules of use; OA articles are governed by the applicable Creative Commons License

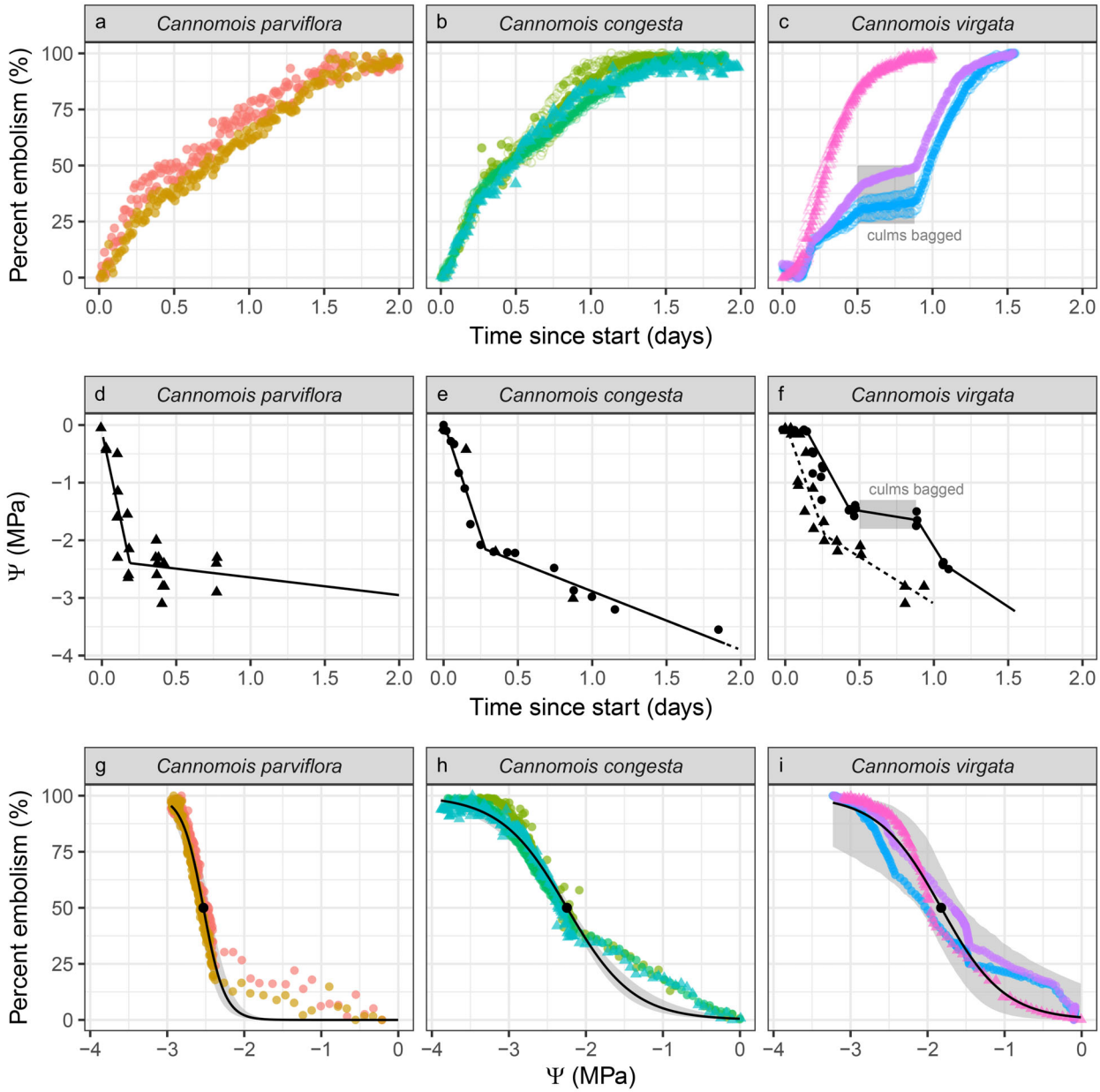

Fig. 4. Pneumatic vulnerability curves for three *Cannomois* species. (a–c) Timeline of percentage embolism, based on air discharge, for each species. Colours represent individual plants, with symbols reflecting measurement round. Open symbols (for *C. congesta* and *C. virgata*) represent individual culms that were averaged per plant (filled symbols). (d–f) Timeline of water potential for each species. Points indicate observed values recorded using the Scholander-type pressure chamber, symbols reflect measurement round, lines indicate interpolated xylem water potential (see Material and Methods for details). (h, i) Xylem vulnerability curves for each species. Coloured symbols as per panel (a–c), solid black lines are mean xylem vulnerability curves, filled black circles indicate the P_{50} values, and the grey shaded areas indicate 95% confidence intervals for each species.

with significant differences found between *C. congesta* and *C. virgata*, but not for *C. parviflora* (Fig. 5c).

Vulnerability to embolism, pressure–volume curves and hydraulic safety margins

All three of the *Cannomois* species were quite vulnerable to embolism, with values for P_{50} ranging between −1.9 MPa (*C. virgata*), −2.3 MPa (*C. congesta*) and −2.4 MPa (*C. parviflora*) (Table 1, Fig. 5). This relative ranking of P_{50} between species corresponded with the values obtained for midday water potential (Ψ_{MD}), turgor loss point (Ψ_{TLP}) and osmotic potential at full turgot (Ψ_O) (Table 1, Fig. 7). Ψ_{TLP} varied significantly between the species, with *C. virgata* having a significantly higher turgor loss point than *C. congesta* and *C. parviflora* (Table 1, Figure S1). A similar result was found for Ψ_O, with significant differences being found between *C. parviflora* and *C. virgata*, whereas RWC_{TLP} was significantly higher for *C. parviflora* than for *C. congesta* and *C. virgata* (Table 1, Figure S1).

14388677, 2024, 4, Downloaded from https://onlinelibrary.wiley.com/doi/10.1111/plb.13644 by University Of Witwatersrand, Wiley Online Library on [22/11/2024]. See the Terms and Conditions (https://onlinelibrary.wiley.com/terms-and-conditions) on Wiley Online Library for rules of use; OA articles are governed by the applicable Creative Commons License

Table 1. Parameters extracted from vulnerability and pressure volume curves as well as measured field water potentials for *Cannomois parviflora*, *C. congesta* and *C. virgata*.

	C. parviflora	*C. congesta*	*C. virgata*	*F* (df)	*P*
P_{50_opt} (MPa)	-2.32 ± 0.14	-2.29 ± 0.06	-1.93 ± 0.05		
P_{12_opt} (MPa)	-2.12 ± 0.14	-1.89 ± 0.04	-1.79 ± 0.03		
P_{88_opt} (MPa)	-2.52 ± 0.15	-2.69 ± 0.09	-2.07 ± 0.09		
P_{50_pneu} (MPa)	-2.53 ± 0.03	-2.25 ± 0.02	-1.82 ± 0.08		
P_{12_pneu} (MPa)	-2.26 ± 0.04	-1.38 ± 0.03	-0.95 ± 0.18		
P_{88_pneu} (MPa)	-2.80 ± 0.02	-3.11 ± 0.06	-2.69 ± 0.13		
Ψ_{TLP} (MPa)	-1.70 ± 0.09^{b}	-1.52 ± 0.02^{b}	-1.28 ± 0.02^{a}	15.9 (2, 6)	**0.004**
Ψ_{o} (MPa)	-1.47 ± 0.15^{b}	-1.11 ± 0.02^{ab}	-0.99 ± 0.04^{a}	8.09 (2, 6)	**0.020**
RWC_{TLP} (%)	96.2 ± 0.73^{b}	90.8 ± 1.0^{a}	89.9 ± 0.96^{a}	16.0 (2, 6)	**0.004**
Ψ_{PD} (MPa)	-0.49 ± 0.14	-0.55 ± 0.08	-0.46 ± 0.05	0.12 (2, 35)	0.888
Ψ_{MD} (MPa)	-1.34 ± 0.12	-1.26 ± 0.09	-1.11 ± 0.14	0.31 (2, 35)	0.734
$HSM_{\Psi MD}$	1.09 ± 0.15	1.01 ± 0.10	0.77 ± 0.15		
$HSM_{\Psi TLP}$	0.73 ± 0.12	0.75 ± 0.04	0.60 ± 0.07		

P_{50_opt}, P_{12_opt}, P_{88_opt} reflect the water potentials at 50%, 12% and 88% embolism measured with the Optical technique. P_{50_pneu}, P_{12_pneu}, P_{88_pneu} reflect the water potentials at 50%, 12% and 88% of maximum air discharge measured with the pneumatic technique. Ψ_{TLP}, turgor loss point; Ψ_{O}, osmotic potential at full turgor; RWC_{TLP}, relative water content at the turgor loss point; Ψ_{PD}, pre-dawn water potential; Ψ_{MD}, midday water potential; $HSM_{\Psi MD}$, hydraulic safety margin (defined as $\Psi_{MD} - P_{50}$); $HSM_{\Psi TLP}$, hydraulic safety margin (defined as $\Psi_{TLP} - P_{50}$). Results from a one-way ANOVA are shown for the pressure volume curve parameters and the field water potential data. Significant differences are shown in bold. Where the ANOVA was significant, letters reflect differences as detected by Tukey HSD post-hoc tests. Results from a two-way ANOVA for the vulnerability curve parameters are shown in Table 2.

Table 2. Results from two-way ANOVA testing for differences between P_{50}, P_{12} and P_{88} by species and method (optical versus pneumatic) with interaction (model: y ~ species × method).

Parameter	Factor	df	*F* value	*P*
P_{50}	Species	2, 14	21.6	5.22E-05
P_{12}	Species	2, 11	29.1	4.1E-05
	Method	1, 11	26.4	3.2E-04
	Species:Method	2, 12	10.3	3.0E-03
P_{88}	Species	2, 13	12.5	9.4E-04
	Method	1, 13	26.4	1.9E-04

Factors and the interaction were dropped from models when not significant following the procedures of Crawley (2012). The simplest model is reported below.

The consistent differences in P_{50}, Ψ_{MD} and Ψ_{TLP} between species resulted in consistent hydraulic safety margins, with the average $HSM_{\Psi MD}$ across species being 0.95 ± 0.1 MPa, and the average $HSM_{\Psi TLP}$ across species being 0.69 ± 0.05 MPa (Table 1, Fig. 7). The P_{12} estimates obtained from the optical method indicated that the onset of embolism occurred approximately 0.43 ± 0.04 MPa after Ψ_{TLP} for all three species (Fig. 6). P_{12} estimates from the pneumatic method were more variable, with $P_{12} < \Psi_{TLP}$ for *C. parviflora*, but $P_{12} > \Psi_{TLP}$ for *C. congesta* and *C. virgata* (Fig. 6).

DISCUSSION

The extent to which aboveground hydraulic traits influence species distributions of graminoids is relatively understudied globally. This is certainly the case for the restios of the Cape Floristic Region (CFR), where strong hydrological niche segregation is seen (Araya *et al.* 2011), as well as a high degree of root lability (Ehmig & Linder 2020), yet little is known about the aboveground hydraulic traits of these species and the extent to which these influence this niche segregation. Here we demonstrate that the optical and pneumatic methods can successfully generate robust estimates of vulnerability to embolism for restios, that will enable future examination of trait–environment relationships in this and other morphologically similar graminoid groups. Doing so allows us to demonstrate that restio occupancy of dry environments involves more than the evolution of highly resistant xylem, suggesting that other aspects of water relations are key to understanding trait–environment relationships in this diverse and ecologically important group (West *et al.* 2012; Skelton *et al.* 2023).

The optical vulnerability method appears to be a reliable method for detecting the dynamics of embolism formation in restio culms. The optical method produced steep sigmoidal curves, with all estimates of vulnerability to embolism (P_{50}, P_{12}, P_{88}) occurring at more negative water potentials than Ψ_{min} and Ψ_{TLP} for all species (Fig. 6a), resulting in positive hydraulic safety margins (Table 2), thereby providing support for the embolism avoidance hypothesis (e.g., Martin-StPaul *et al.* 2017; Skelton *et al.* 2021). The relative rankings of the estimates of vulnerability to embolism (P_{50}, P_{12}, P_{88}) were correlated with the relative values of Ψ_{min} and Ψ_{TLP}, with the more mesic *C. virgata* appearing more vulnerable to embolism, and with higher Ψ_{min} and Ψ_{TLP} than the dryland *C. congesta* and *C. parviflora* (Fig. 7a). We could not distinguish between the two dryland species in this study, and increased sample size will be necessary if attempting to detect differences between such similar species in future.

The P_{50} estimated by the pneumatic method was very consistent with that from the optical method (Fig. 6). However, there

14388677, 2024, 4, Downloaded from https://onlinelibrary.wiley.com/doi/10.1111/plb.13644 by University Of Witwatersrand, Wiley Online Library on [22/11/2024]. See the Terms and Conditions (https://onlinelibrary.wiley.com/terms-and-conditions) on Wiley Online Library for rules of use; OA articles are governed by the applicable Creative Commons License

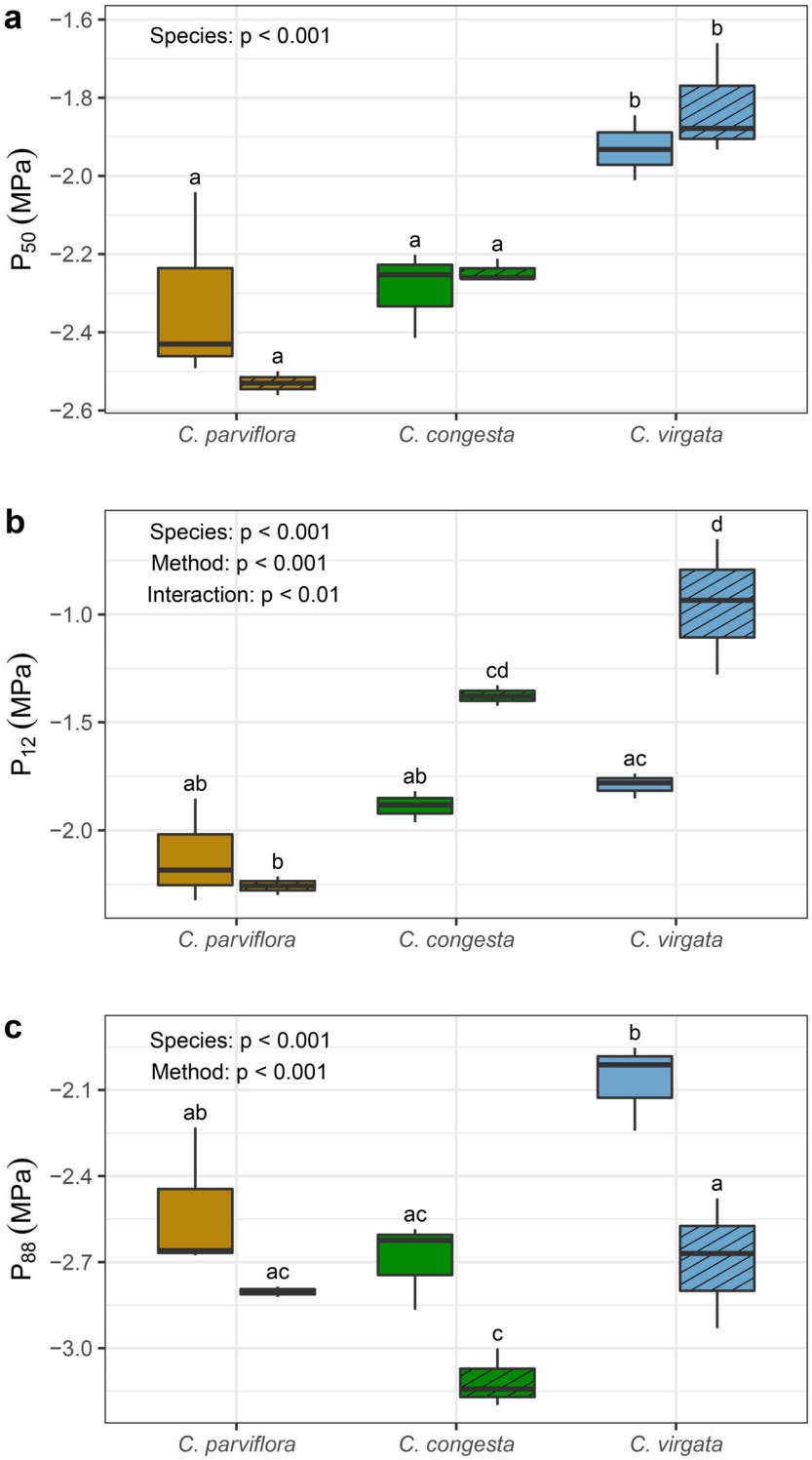

Fig. 5. Comparison of critical water potential thresholds, P_{50} (a), P_{12} (b) and P_{88} (c), for three species of *Cannomois* measured by the optical (solid boxes) and pneumatic (hatched boxes) vulnerability methods. Horizontal bars represent the minimum and maximum (outer bars connected by dashed lines), the median (inner, thick lines), and the first quartile and third quartile in the dataset of each species. Open circles represent outliers. Significant factors (two-way ANOVA) are shown in each panel, with letters reflecting significant differences between treatments as determined by Tukey HSD post-hoc tests.

was disagreement between the methods regarding P_{12} and P_{88} (Fig. 6). Recent work indicates that sap residue in cut xylem conduits can result in early gas discharge, influencing the slope of vulnerability curves produced by the pneumatic method for some woody species (Miranda *et al.* 2023). As demonstrated by Miranda *et al.* (2023), this early gas discharge only occurred at

14388677, 2024, 4, Downloaded from https://onlinelibrary.wiley.com/doi/10.1111/plb.13644 by University Of Witwatersrand, Wiley Online Library on [22/11/2024]. See the Terms and Conditions (https://onlinelibrary.wiley.com/terms-and-conditions) on Wiley Online Library for rules of use; OA articles are governed by the applicable Creative Commons License

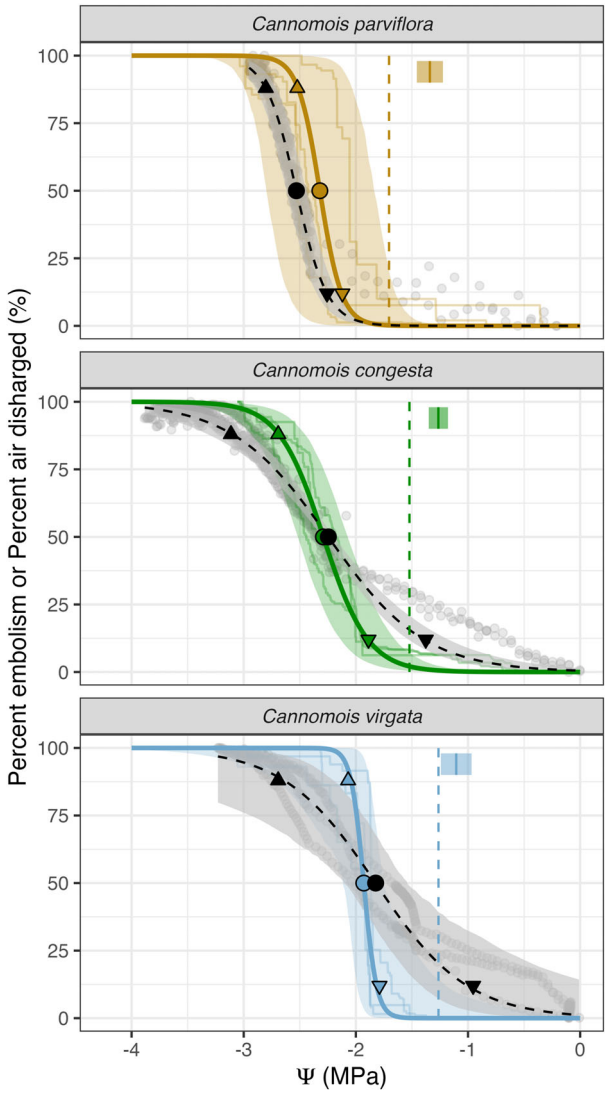

Fig. 6. Methods comparison of the optical and pneumatic vulnerability curves for three species of *Cannomois*. Thick solid coloured lines represent the mean optical vulnerability curve, with 95% confidence intervals shown by coloured shading and individual culms shown by thin solid lines. Mean pneumatic vulnerability curves are represented by dashed, black lines, with 95% confidence intervals shown by grey shading, and individual culms shown by grey symbols. Critical water potential thresholds are shown on the mean vulnerability curves as filled circles (P_{50}), down-facing triangles (P_{12}) and upward-facing triangles (P_{88}). Also shown is the water potential associated with turgor loss of culms (vertical coloured dashed lines) and minimum field xylem water potential (coloured horizontal bars reflecting range, with vertical line indicating the mean).

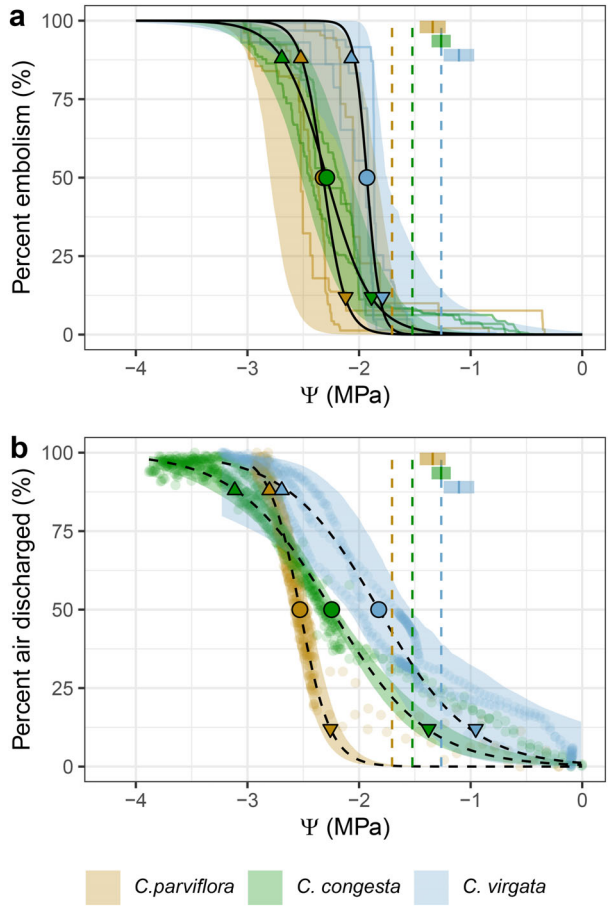

Fig. 7. Xylem vulnerability curves for the three species generated using the optical (a) and the pneumatic (b) vulnerability techniques. In each panel the solid black lines are mean xylem vulnerability curves for each species and the shading indicates the 95% confidence intervals. Critical water potential thresholds are shown on the mean vulnerability curves as filled circles (P_{50}), down-facing triangles (P_{12}) and upward-facing triangles (P_{88}). Also shown is the water potential associated with turgor loss of culms (vertical coloured dashed lines) and minimum field xylem water potential (coloured horizontal bars reflecting range, with vertical line indicating the mean).

water potentials greater than turgor loss point and was not related to embolism formation. Correcting for this early gas discharge resulted in strong agreement between the pneumatic and optical methods. A similar artefact may have been present in our measurements on restios. All our pneumatic curves displayed early gas discharge at odds with the onset of embolism shown by the optical curves (Fig. 6). It is possible that this early gas discharge resulted from sap residue in cut xylem conduits, as well as from the extensive parenchymatous tissue surrounding the vascular bundles, prior to the onset of the turgor loss point. Additionally, potential changes in discharge tube volume during culm desiccation might influence the calculation of air discharge if not properly quantified. These factors were not directly tested in this study, and remain future research directions to explore. Nevertheless, despite possible contributions of non-embolism related gas discharge, pneumatic estimates of P_{50} can be robust (Pereira *et al.* 2016), as appears to be the case here, given the similarity between the two methods (Fig. 6). As such, we consider the pneumatic method to be a useful way to estimate P_{50} for these species. Additionally, future methods developments will no doubt improve pneumatic estimates of P_{50}, P_{12} and P_{88}.

Future studies might also examine hypotheses linking inter-culm (or intra-individual) variability in vulnerability to individual survival in the Restionaceae. High inter-leaf variability in xylem resistance to embolism in *Persea* has been linked with heterogeneity in drought-induced leaf mortality across the canopy, which may act as a buffer against complete canopy death during prolonged drought (Cardoso *et al.* 2020). We have observed patchy dieback across *Cannomois* individuals during

14388677, 2024, 4, Downloaded from https://onlinelibrary.wiley.com/doi/10.1111/plb.13644 by University Of Witwatersrand, Wiley Online Library on [22/11/2024]. See the Terms and Conditions (https://onlinelibrary.wiley.com/terms-and-conditions) on Wiley Online Library for rules of use; OA articles are governed by the applicable Creative Commons License

prolonged dry periods (see Plate 3.4, Skelton 2014) and future studies might examine if the inter-culm variation in vulnerability, seen most noticeably with the optical method (Fig. 3), correlates with these phenomena in the field.

Our estimates of P_{50} for our three *Cannomois* species were between −1.9 and −2.4 MPa (Table 2), which is suggestive of a relatively high vulnerability to embolism for these perennial graminoids, growing in seasonally dry environments. Previous estimates of P_{50} for graminoids range widely between −0.5 and −7.6 MPa (e.g., Holloway-Phillips & Brodribb 2011; Skelton *et al.* 2015; Lens *et al.* 2016; Ocheltree *et al.* 2016; Johnson *et al.* 2018). However, these studies used a wide variety of methods, which renders direct comparison potentially challenging. Directly comparable studies for graminoids, using the optical technique, have measured P_{50} of between −2.21 and −2.87 MPa for wheat (Johnson *et al.* 2018; Corso *et al.* 2020), and between −4.4 and −6.1 MPa for five different pasture grasses (Jacob *et al.* 2022).

Our finding of greater vulnerability to embolism in three perennial restio species than that found in an annual crop species, such as wheat, demands explanation. One possible explanation could be that individual culms are not built to endure negative water potentials through the dry season, having negative safety margins and being effectively drought-deciduous. Several lines of evidence indicate that this is not the case in most Restionaceae species, including *Cannomois*. While a previous study found negative safety margins for two species of restios (*H. aristata* and *C. congesta*) (Skelton *et al.* 2015), the estimates of P_{50} for these species were produced using air-injection and hydraulic methods that resulted in exponential curves that most likely overestimated vulnerability (e.g., Cochard *et al.* 2013). Our study supports this by demonstrating sigmoidal vulnerability curves, with positive safety margins for these species, which we consider a considerable advance in our ability to accurately measure vulnerability curves for these species. Furthermore, *Cannomois* are evergreen perennials, retaining functional culms all year round (Linder 2018; Skelton *et al.* 2023). They do not have sterile culms, which may follow more acquisitive strategies, retaining only fertile culms which are more conservative (Ehmig *et al.* 2019). Individual culms live for several years, commencing growth before the start of the wet winter (van Blerk *et al.* 2022), with the female plants of *C. congesta* holding a single nut for 2 years at the distal tip of the culm before it is mature and released (van Blerk *et al.* 2017). Thus, inability to survive at least one dry season would result in considerable fitness costs for these plants. Drought-deciduousness is also extremely rare in the fynbos, presumably due to the paucity of nutrients, which make an evergreen, sclerophyllous strategy most adaptive.

Another possible explanation for the relatively high vulnerability to embolism is that these restios are able to avoid negative water potentials in their culms throughout the dry season, thereby maintaining a positive hydraulic safety margin and avoiding embolism in the culms. This study, as well as previous field observations on restios, support this explanation. In this study, the onset of embolism occurred after both the Ψ_{TLP} and Ψ_{min} for all species (Fig. 6). While there are no comparable measurements of Ψ_{TLP} in the literature, our measurements of Ψ_{min} are comparable to previous studies. Minimum water potentials for *Cannomois acuminata* (now *C. parviflora*) were measured as >−1.9 MPa between October to May at the same field site used for this study (Miller *et al.* 1984; von Willert *et al.* 1989). Similarly, a multi-year field ecophysiological investigation of the shallow-rooted *C. congesta* found that Ψ_{min} never fell below −2 MPa, even in a particularly dry year, typically remaining >−1.2 MPa throughout the year (Skelton *et al.* 2023). Gas exchange and sap flow were also maintained in these culms throughout the year, at relatively low levels (Skelton *et al.* 2013; Skelton *et al.* 2023), most likely sustained by the uptake of the regular dew and cloud moisture events during rain-free periods (Skelton *et al.* 2023). This combination of low rates of gas exchange with regular moisture uptake may enable the success of these leafless culms through the relatively mild summers typical of the Cape mountain fynbos.

The ability of restios to intercept and trap cloud moisture (Marloth 1903, 1905; Nagel 1956), has the potential to alleviate summer drought stress in areas receiving frequent bouts of summer cloud. This was demonstrated by an in-situ drought experiment in mountain fynbos, where all summer rainfall, but not cloud moisture, was removed from natural plots containing proteas, ericas and restios (West *et al.* 2012). Despite having no summer rainfall, water potentials in the restios (*Hypodiscus aristatus* and *Staberoha cernua*) never fell below −2 MPa, presumably because of the regular uptake of cloud moisture that would frequently wet the foliage over the summer, whereas co-occurring shallow-rooted *Erica* species experienced water potentials down to −10 MPa. As a result, there was no drought impact on the restios, whereas *Erica* species suffered dieback and mortality (West *et al.* 2012).

The ability to obtain robust estimates of vulnerability to embolism for reed-like graminoids should enable exploration of the importance of water relations parameters in the restios and other morphologically similar groups. For the restios, there are several pressing lines for investigation. The 350 species of restios occur across the full hydrological range in the CFR. Yet to date, only a handful of species have received close attention, mostly in relatively mesic mountain fynbos (Miller *et al.* 1984; von Willert *et al.* 1989; West *et al.* 2012; Skelton *et al.* 2023). It is of particular interest to determine the hydraulic safety margins in restios across their full hydrologic range, and the extent to which future drought may impact this ecologically important component of the CFR. This is a pressing research agenda, given the strong likelihood of increasingly severe drought in the region (IPCC 2022). There is also interesting work to be done in uncovering the hydraulic basis for the strong hydrologic niche segregation seen in this group (Araya *et al.* 2011), particularly in the context of increased groundwater abstraction from the CFR to meet human water needs (February *et al.* 2004). Lastly, there is considerable interest in the role that hydrologic refugia (Mclaughlin *et al.* 2017) may have played in the evolution of the Cape Flora. The ability to add robust hydraulic traits to restio distribution and phylogeny should considerably aid this research.

ACKNOWLEDGEMENTS

The authors wish to acknowledge the Du Plessis family for access to Jonaskop, and Cape Nature (Permit number 0052-AAA008-00008 and CN32-28-14428) for allowing access to the Jonaskop, Cederberg and Jonkershoek study sites. Financial support was received from a FLAIR Fellowship from the Royal Society and the African Academy of Sciences awarded to RPS (Award number FLR\R1\191609). The FLAIR Fellowship

14388677, 2024, 4, Downloaded from https://onlinelibrary.wiley.com/doi/10.1111/plb.13644 by University Of Witwatersrand, Wiley Online Library on [22/11/2024]. See the Terms and Conditions (https://onlinelibrary.wiley.com/terms-and-conditions) on Wiley Online Library for rules of use; OA articles are governed by the applicable Creative Commons License

Programme is a partnership between the African Academy of Sciences and the Royal Society funded by the UK Government's Global Challenges Research Fund. The authors acknowledge Brad Ripley and Liam Reynolds for assistance in developing the pneumatron method.

AUTHOR CONTRIBUTIONS

AGW and RPS designed the study. AGW and RPS performed the experiments and collected all the data. KA assisted in developing the optical method for use on restios. JvB provided anatomical sections. Data were analysed by AGW, RPS and JvB. AGW wrote the manuscript with revisions from RPS, JvB and KA.

SUPPORTING INFORMATION

Additional supporting information may be found online in the Supporting Information section at the end of the article.

Figure S1. (a) Pressure-volume curves for three species of *Cannomois*.

REFERENCES

Adams H.D., Zeppel M.J.B., Anderegg W.R.L., Hartmann H., Landhäusser S.M., Tissue D.T., Huxman T.E., Hudson P.J., Franz T.E., Allen C.D., Anderegg L.D., Barron-Gafford G.A., Beerling D.J., Breshears D.D., Brodribb T.J., Bugmann H., Cobb R.C., Collins A.D., Dickman L.T., Duan H., Ewers B.E., Galiano L., Galvez D.A., Garcia-Forner N., Gaylord M.L., Germino M.J., Gessler A., Hacke U.G., Hakamada R., Hector A., Jenkins M.W., Kane J.M., Kolb T.E., Law D.J., Lewis J.D., Limousin J.-M., Love D.M., Macalady A.K., Martínez-Vilalta J., Mencuccini M., Mitchell P.J., Muss J.D., O'Brien M.J., O'Grady A.P., Pangle R.E., Pinkard E.A., Piper F.I., Plaut J.A., Pockman W.T., Quirk J., Reinhardt K., Ripullone F., Ryan M.G., Sala A., Sevanto S., Sperry J.S., Vargas R., Vennetier M., Way D.A., Xu C., Yepez E.A., McDowell N.G. (2017) A multi-species synthesis of physiological mechanisms in drought-induced tree mortality. *Nature Ecology & Evolution*, **1**, 1285–1291.

Anderegg W.R.L., Berry J.A., Smith D.D., Sperry J.S., Anderegg L.D.L., Field C.B. (2012) The roles of hydraulic and carbon stress in a widespread climate-induced forest die-off. *roceedings of the National Academy of Sciences of the United States of America*, **109**, 233–237.

Araya Y.N., Silvertown J., Gowing D.J. (2012) Do niche-structured plant communities exhibit phylogenetic conservatism? A test case in an endemic clade. *Journal of Ecology*, **100**, 1434–1439.

Araya Y.N., Silvertown J., Gowing D.J., McConway K.J., Peter L.H., Midgley G. (2011) A fundamental, eco-hydrological basis for niche segregation in plant communities. *New Phytologist*, **189**, 253–258.

Bartlett M.K., Scoffoni C., Sack L. (2012) The determinants of leaf turgor loss point and prediction of drought tolerance of species and biomes: a global meta-analysis. *Ecology Letters*, **15**, 393–405.

Bell T.L., Stock W.D., Linder H.P. (2000) Ecophysiological investigations of the distribution of Poaceae and Restionaceae in the cape floristic region, South Africa, *Grasses: Systematics and evolution*. CSIRO, Melbourne, Australia, pp 267–278.

Bergh N.G., Verboom G., Rouget M., Cowling R.M. (2014) Vegetation types of the greater cape floristic region, *Fynbos: Ecology, evolution, and conservation of a megadiverse region*. Oxford University Press, Oxford, UK, pp 1–25.

Bond P., Goldblatt P. (1984) Plants of the Cape Flora: a descriptive catalogue. *Journal of South African Botany*, **7**, 304–306.

Bond W.J., Midgley G.F. (2012) Carbon dioxide and the uneasy interactions of trees and savannah grasses. *Philosophical Transactions of the Royal Society, B: Biological Sciences*, **367**, 601–612.

Born J., Linder H.P. (2018) Water availability, fundamental niches and realized niches: a case study from the Cape flora. *Austral Ecology*, **6**, 696–705.

Briggs B.G., Linder H.P. (2009) A new subfamilial and tribal classification of Restionaceae (Poales). *Telopea*, **12**, 333–345.

Brodersen C.R., Roddy A.B., Wason J.W., McElrone A.J. (2019) Functional status of xylem through time. *Annual Review of Plant Biology*, **70**, 407–433.

Brodribb T., Brodersen C.R., Carriqui M., Tonet V., Rodriguez D.C., McAdam S. (2021) Linking xylem network failure with leaf tissue death. *New Phytologist*, **232**, 68–79.

Brodribb T.J., Carriqui M., Delzon S., Lucani C. (2017) Optical measurement of stem xylem vulnerability. *Plant Physiology*, **174**, 2054–2061.

Brodribb T.J., Powers J., Cochard H., Choat B. (2020) Hanging by a thread? Forests and drought. *Science*, **368**, 261–266.

Brodribb T.J., Skelton R.P., MCAdam S.A.M., Bienaimé D., Lucani C.J., Marmottant P. (2016) Visual quantification of embolism reveals leaf vulnerability to hydraulic failure. *New Phytologist*, **209**, 1403–1409.

Campbell B.M. (1983) Montane plant environments in the fynbos biome. *Bothalia*, **14**, 283–298.

Cao K.-F., Yang S.-J., Zhang Y.-J., Brodribb T.J. (2012) The maximum height of grasses is determined by roots: root pressure determines height in bamboo. *Ecology Letters*, **15**, 666–672.

Cardoso A.A., Batz T.A., McAdam S.A.M. (2020) Xylem embolism resistance determines leaf mortality during drought in *Persea americana*. *Plant Physiology*, **182**, 547–554.

Choat B., Brodribb T.J., Brodersen C.R., Duursma R.A., López R., Medlyn B.E. (2018) Triggers of tree mortality under drought. *Nature*, **558**, 531–539.

Cochard H., Badel E., Herbette S., Delzon S., Choat B., Jansen S. (2013) Methods for measuring plant vulnerability to cavitation: a critical review. *Journal of Experimental Botany*, **64**, 4779–4791.

Corso D., Delzon S., Lamarque L.J., Cochard H., Torres-Ruiz J.M., King A., Brodribb T. (2020) Neither xylem collapse, cavitation, or changing leaf conductance drive stomatal closure in wheat. *Plant, Cell & Environment*, **43**, 854–865.

Craine J.M., Ocheltree T.W., Nippert J.B., Towne E.G., Skibbe A.M., Kembel S.W., Fargione J.E. (2013) Global diversity of drought tolerance and grassland climate-change resilience. *Nature Climate Change*, **3**, 63–67.

Crawley M. (2012) Analysis of variance, *The R book*. John Wiley & Sons, Chichester, UK, pp 498–536.

Domec J.-C., Gartner B.L. (2001) Cavitation and water storage capacity in bole xylem segments of mature and young Douglas-fir trees. *Trees*, **15**, 204–214.

Ehmig M., Coiro M., Linder H.P. (2019) Ecophysiological strategy switch through development in heteroblastic species of mediterranean ecosystems – An example in the African Restionaceae. *Annals of Botany*, **123**, 611–623.

Ehmig M., Linder H.P. (2020) Unexpected diversity and evolutionary lability in root architectural ecomorphs in the rushes of the hyperdiverse Cape flora. *New Phytologist*, **227**, 216–231.

Fay P.A., Carlisle J.D., Knapp A.K., Blair J.M., Collins S.L. (2003) Productivity responses to altered rainfall patterns in a C4 -dominated grassland. *Oecologia*, **137**, 245–251.

February E.C., Bond W.J., Taylor R., Newton R. (2004) Will water abstraction from the Table Mountain aquifer threaten endemic species? A case study at Cape Point, Cape Town. *South African Journal of Science*, **100**, 253.

February E.C., Higgins S.I., Bond W.J., Swemmer L. (2013) Influence of competition and rainfall manipulation on the growth responses of savanna trees and grasses. *Ecology*, **94**, 1155–1164.

Goldblatt P. (1978) An analysis of the flora of southern Africa: its characteristics, relationships, and orgins. *Annals of the Missouri Botanical Garden*, **65**, 369–436.

Goud E.M., Touchette S., Strachan I.B., Strack M. (2022) Graminoids vary in functional traits, carbon dioxide and methane fluxes in a restored peatland: implications for modelling carbon storage. *Journal of Ecology*, **110**, 2105–2117.

Hoffman M.T., Moll E.J., Boucher C. (1987) Post-fire succession at Pella, a south African lowland fynbos site. *South African Journal of Botany*, **53**, 370–374.

Holloway-Phillips M.-M., Brodribb T.J. (2011) Minimum hydraulic safety leads to maximum water-use efficiency in a forage grass: minimum hydraulic safety, maximum water-use efficiency. *Plant, Cell & Environment*, **34**, 302–313.

Huber M., Linder H.P. (2012) The evolutionary loss of aerenchyma limits both realized and fundamental ecohydrological niches in the Cape reeds (Restionaceae). *Journal of Ecology*, **100**, 1338–1348.

IPCC (2022) *Climate change 2021: the physical science basis. Contribution of working group I to the sixth assessment report of the intergovernmental panel on climate change*. Cambridge University Press, Cambridge, UK.

Jacob V., Choat B., Churchill A.C., Zhang H., Barton C.V.M., Krishnananthaselvan A., Post A.K., Power S.A., Medlyn B.E., Tissue D.T. (2022) High safety margins to drought-induced hydraulic failure found in five pasture grasses. *Plant, Cell & Environment*, **45**, 1631–1646.

Johnson K.M., Jordan G.J., Brodribb T.J. (2018) Wheat leaves embolized by water stress do not recover function upon rewatering. *Plant, Cell & Environment*, **41**, 2704–2714.

Jurjavcic N., Harrison S., Wolf A. (2002) Abiotic stress, competition, and the distribution of the native

14388677, 2024, 4, Downloaded from https://onlinelibrary.wiley.com/doi/10.1111/plb.13644 by University Of Witwatersrand, Wiley Online Library on [22/11/2024]. See the Terms and Conditions (https://onlinelibrary.wiley.com/terms-and-conditions) on Wiley Online Library for rules of use; OA articles are governed by the applicable Creative Commons License

annual grass *Vulpia microstachys* in a mosaic environment. *Oecologia*, **130**, 555–562.
Karp A.T., Faith J.T., Marlon J.R., Staver A.C. (2021) Global response of fire activity to late quaternary grazer extinctions. *Science*, **374**, 1145–1148.
Kassambara A. (2020) ggpubr: "ggplot2" based publication ready plots.
Knapp A.K., Fay P.A., Blair J.M., Collins S.L., Smith M.D., Carlisle J.D., Harper C.W., Danner B.T., Lett M.S., McCarron J.K. (2002) Rainfall variability, carbon cycling, and plant species diversity in a Mesic grassland. *Science*, **298**, 2202–2205.
Lens F., Picon-Cochard C., Delmas C.E.L., Signarbieux C., Buttler A., Cochard H., Jansen S., Chauvin T., Doria L.C., Del Arco M., Delzon S. (2016) Herbaceous angiosperms are not more vulnerable to drought-induced embolism than angiosperm trees. *Plant Physiology*, **172**, 661–667.
Linder H.P. (2018) African Restionaceae, electronic dataset. Available from https://www.systbot.uzh.ch/en/Bestimmungsschluessel/Restionaceae.html (accessed July 2022).
Marloth R. (1903) Results of experiments on Table Mountain for ascertaining the amount of moisture deposited from the south-east clouds. *Transactions of the South African Philosophical Society*, **14**, 403–408.
Marloth R. (1905) Results of further experiments on Table Mountain for ascertaining the amount of moisture deposited from the south-east clouds. *Transactions of the South African Philosophical Society*, **16**, 97–105.
Martin-StPaul N., Delzon S., Cochard H. (2017) Plant resistance to drought depends on timely stomatal closure. *Ecology Letters*, **20**, 1437–1447.
McDowell N., Pockman W.T., Allen C.D., Breshears D.D., Cobb N., Kolb T., Plaut J., Sperry J., West A., Williams D.G., Yepez E.A. (2008) Mechanisms of plant survival and mortality during drought: why do some plants survive while others succumb to drought? *New Phytologist*, **178**, 719–739.
Mclaughlin B.C., Ackerly D.D., Klos P.Z., Natali J., Dawson T.E., Thompson S.E. (2017) Hydrologic refugia, plants, and climate change. *Global Change Biology*, **23**, 2941–2961.
Miller J.M., Miller P.C., Miller P.M. (1984) Leaf conductances and xylem pressure potentials in fynbos plant species. *South African Journal of Science*, **80**, 381–385.
Miranda M.T., Pereira L., Pires G.S., Guan X., Silva L.M., Kreinert S., Machado E.C., Jansen S., Ribeiro R.V. (2023) Xylem sap residue in cut-open conduits can affect gas discharge in pneumatic experiments.
Muggeo V.M.R. (2008) Segmented: an R package to fit regression models with broken-line relationships. *R News*, **8**, 20–25.
Nagel J.F. (1956) Fog precipitation on Table Mountain. *Quarterly Journal of the Royal Meteorological Society*, **82**, 452–460.
Nicotra A., Sack L., Santiago L., Cornwell W. (2010) PrometheusWiki: protocols, methods, explanations and updated standards for ecological and environmental plant physiology.
Ocheltree T.W., Mueller K.M., Chesus K., LeCain D.R., Kray J.A., Blumenthal D.M. (2020) Identification of suites of traits that explains drought resistance and phenological patterns of plants in a semi-arid grassland community. *Oecologia*, **192**, 55–66.
Ocheltree T.W., Nippert J.B., Prasad P.V.V. (2016) A safety vs efficiency trade-off identified in the hydraulic pathway of grass leaves is decoupled from photosynthesis, stomatal conductance and precipitation. *New Phytologist*, **210**, 97–107.
Paligi S.S., Link R.M., Isasa E., Bittencourt P., Cabral J.S., Jansen S., Oliveira R.S., Pereira L., Schuldt B. (2023) Assessing the agreement between the pneumatic and the flow-centrifuge method for estimating xylem safety in temperate diffuse-porous tree species. *Plant Biology*, **25**, 1171–1185.
Pammenter N.W., van der Willigen C. (1998) A mathematical and statistical analysis of the curves illustrating vulnerability of xylem to cavitation. *Tree Physiology*, **18**, 589–593.
Pereira L., Bittencourt P.R.L., Oliveira R.S., Junior M.B.M., Barros F.V., Ribeiro R.V., Mazzafera P. (2016) Plant pneumatics: stem air flow is related to embolism – New perspectives on methods in plant hydraulics. *New Phytologist*, **211**, 357–370.
Pereira L., Bittencourt P.R.L., Pacheco V.S., Miranda M.T., Zhang Y., Oliveira R.S., Groenendijk P., Machado E.C., Tyree M.T., Jansen S., Rowland L., Ribeiro R.V. (2020) The Pneumatron: an automated pneumatic apparatus for estimating xylem vulnerability to embolism at high temporal resolution. *Plant, Cell & Environment*, **43**, 131–142.
R Core Team (2022) *R: a language and environment for statistical computing*. R Foundation for Statistical Computing, Vienna, Austria.
Rebelo A.G., Boucher C., Helme N., Mucina L., Rutherford M.C. (2006) Fynbos Biome, *The vegetation of South Africa, Lesotho and Swaziland*. South African National Biodversity Institute, Pretoria, South Africa, pp 53–218.
Silvertown J., Araya Y., Gowing D. (2015) Hydrological niches in terrestrial plant communities: a review. *Journal of Ecology*, **103**, 93–108.
Silvertown J., Dodd M.E., Gowing D.J.G., Mountford J.O. (1999) Hydrologically defined niches reveal a basis for species richness in plant communities. *Nature*, **400**, 61–63.
Skelton R.P. (2014) The role of hydraulic strategies in understanding the response of fynbos to drought PhD Thesis. University of Cape Town, South Africa.
Skelton R.P., Anderegg L.D.L., Diaz J., Kling M.M., Papper P., Lamarque L.J., Delzon S., Dawson T.E., Ackerly D.D. (2021) Evolutionary relationships between drought-related traits and climate shape large hydraulic safety margins in western north American oaks. *Proceedings of the National Academy of Sciences of the United States of America*, **118**, e2008987118.
Skelton R.P., Dawson T.E., Thompson S.E., Shen Y., Weitz A.P., Ackerly D. (2018) Low vulnerability to xylem embolism in leaves and stems of North American oaks. *Plant Physiology*, **177**(3), 1066–1077. https://doi.org/10.1104/pp.18.00103
Skelton R.P., West A.G., Buttner D., Dawson T.E. (2023) Consistent responses to moisture stress despite diverse growth forms within mountain fynbos communities. *Oecologia*, **201**, 323–339.
Skelton R.P., West A.G., Dawson T.E. (2015) Predicting plant vulnerability to drought in biodiverse regions using functional traits. *Proceedings of the National Academy of Sciences of the United States of America*, **112**, 5744–5749.
Skelton R.P., West A.G., Dawson T.E., Leonard J.M. (2013) External heat-pulse method allows comparative sapflow measurements in diverse functional types in a Mediterranean-type shrubland in South Africa. *Functional Plant Biology*, **40**, 1076–1087.
Staver A.C., Archibald S., Levin S. (2011) Tree cover in sub-Saharan Africa: rainfall and fire constrain forest and savanna as alternative stable states. *Ecology*, **92**, 1063–1072.
Staver A.C., Wigley-Coetsee C., Botha J. (2019) Grazer movements exacerbate grass declines during drought in an African savanna. *Journal of Ecology*, **107**, 1482–1491.
Swemmer A.M., Knapp A.K., Smith M.D. (2006) Growth responses of two dominant C4 grass species to altered water availability. *International Journal of Plant Sciences*, **167**, 1001–1010.
Trabi C.L., Pereira L., Guan X., Miranda M.T., Bittencourt P.R.L., Oliveira R.S., Ribeiro R.V., Jansen S. (2021) A user manual to measure gas diffusion kinetics in plants: pneumatron construction, operation, and data analysis. *Frontiers in Plant Science*, **12**, 633595.
Tyree M.T., Sperry J.S. (1989) Vulnerability of xylem to cavitation and embolism. *Annual Review of Plant Physiology and Plant Molecular Biology*, **40**, 19–36.
van Blerk J.J., West A.G., Midgley J.J. (2017) Restio culm felling is a consequence of pre-dispersal seed predation by the rodent *Rhabdomys pumilio* in the fynbos. *South African Journal of Botany*, **112**, 123–127.
van Blerk J.J., West A.G., Skelton R.P., Midgley J.J. (2022) Phenological asynchrony between sexes of Restionaceae can explain culm $\delta^{13}C$ differences. *Austral Ecology*, **47**, 1200–1207.
Van Sundert K., Arfin Khan M.A.S., Bharath S., Buckley Y.M., Caldeira M.C., Donohue I., Dubbert M., Ebeling A., Eisenhauer N., Eskelinen A., Finn A., Gebauer T., Haider S., Hansart A., Jentsch A., Kübert A., Nijs I., Nock C.A., Nogueira C., Porath-Krause A.J., Radujković D., Raynaud X., Risch A.C., Roscher C., Scherer-Lorenzen M., Schuchardt M.A., Schütz M., Siebert J., Sitters J., Spohn M., Virtanen R., Werner C., Wilfahrt P., Vicca S. (2021) Fertilized graminoids intensify negative drought effects on grassland productivity. *Global Change Biology*, **27**, 2441–2457.
von Willert D.J., Herppich M., Miller J.M. (1989) Photosynthetic characteristics and leaf water relations of mountain fynbos vegetation in the Cedarberg area (South Africa). *South African Journal of Botany*, **55**, 288–298.
West A.G., Dawson T.E., February E.C., Midgley G.F., Bond W.J., Aston T.L. (2012) Diverse functional responses to drought in a Mediterranean-type shrubland in South Africa. *New Phytologist*, **195**, 396–407.
Wickham H. (2016) *ggplot2: elegant graphics for data analysis*. Springer, New York, USA.
Wickham H., Averick M., Bryan J., Chang W., McGowan L.D., François R., Grolemund G., Hayes A., Henry L., Hester J., Kuhn M., Pedersen T., Miller E., Bache S., Müller K., Ooms J., Robinson D., Seidel D., Spinu V., Takahashi K., Vaughan D., Wilke C., Woo K., Yutani H. (2019) Welcome to the tidyverse. *Journal of Open Source Software*, **4**, 1686.
Yang D., Pereira L., Peng G., Ribeiro R.V., Kaack L., Jansen S., Tyree M.T. (2022) A unit pipe pneumatic model to simulate gas kinetics during measurements of embolism in excised angiosperm xylem. *Tree Physiology*, **43**, 88–101.
Zhou Y., Singh J., Butnor J.R., Coetsee C., Boucher P.B., Case M.F., Hockridge E.G., Davies A.B., Staver A.C. (2022) Limited increases in savanna carbon stocks over decades of fire suppression. *Nature*, **603**, 445–449.

14388677, 2024, 4, Downloaded from https://onlinelibrary.wiley.com/doi/10.1111/plb.13644 by University Of Witwatersrand, Wiley Online Library on [22/11/2024]. See the Terms and Conditions (https://onlinelibrary.wiley.com/terms-and-conditions) on Wiley Online Library for rules of use; OA articles are governed by the applicable Creative Commons License